EurJIC European Journal of Inorganic Chemistry

ChemPubSoc Europe

FULL PAPER

DOI:10.1002/ejic.201500008

Monoclinic Copper(I) Selenide Nanocrystals and Copper(I) Selenide/Palladium Heterostructures: Synthesis, Characterization, and Surface-Enhanced Raman Scattering Performance

Long Zhang,[a] Shulin Zhao,[a] Yafei Li,[a] Yaqian Lan,[a] Min Han,[a] Zhihui Dai,*[a] and Jianchun Bao*[a]

Keywords: Nanocrystals / Copper / Selenium / Palladium / Synthetic methods / Raman spectroscopy

We have developed a simple and facile approach to the fabrication of monoclinic Cu_2Se nanocrystals and Cu_2Se/Pd heterostructures. $[(C_2H_5)_4N]_2[CuCl_4]$ was chosen as the copper source and SeO_2/terpineol was used as the Se^{-II} precursor for the generation of hexagonal CuSe and cubic $Cu_{2-x}Se$ through the "hot-injection" and "one-pot" methods, respectively. Both CuSe and $Cu_{2-x}Se$ could be further transformed into monoclinic Cu_2Se through heat treatment with trioctylphosphine (TOP) at 220 °C. Cu_2Se/Pd as well as CuSe/Pd and $Cu_{2-x}Se$/Pd were readily obtained by simply mixing copper selenides and $Pd(NO_3)_2$ in a 2-propanol solution. The Pd nanoparticles were distributed on the surface of the copper selenides. The effect of certain reaction parameters on the formation of copper selenides was studied. The amount of terpineol used played an important role in the phase-selective synthesis of CuSe and $Cu_{2-x}Se$. The surface-enhanced Raman scattering (SERS) performance of the heterostructures was investigated with 4-mercaptopyridine (4-Mpy) as a probe molecule. Owing to the strong synergistic effects between Cu_2Se and Pd, Cu_2Se/Pd showed greater SERS performance than pure Pd or Cu_2Se. Moreover, compared to those of CuSe/Pd and $Cu_{2-x}Se$/Pd, Cu_2Se/Pd exhibited the highest SERS sensitivity to 4-Mpy with a detection limit as low as 1.0×10^{-9} M, which revealed its phase- and composition-dependent characteristics. This Cu_2Se/Pd heterostructure exhibits potential applications in the chemical and biological sensing fields.

Introduction

Micro- and nanoscaled transition-metal chalcogenides (TMCs) have attracted much attention because of their unique chemical and physical properties, which allow for widespread applications in energy devices,[1–3] sensors,[4,5] thermoelectric devices,[6,7] and memory devices.[8,9] Among the various TMCs, copper selenides (Cu_xSe, x = 1–2) are very important semiconductors and exist in a wide range of compositions (CuSe, Cu_2Se, $CuSe_2$, Cu_3Se_2, $Cu_{2-x}Se$ etc.) and crystallographic forms (monoclinic, cubic, tetragonal, hexagonal, etc.).[10] For stoichiometric Cu_2Se, there are five types of crystal phase, namely, the cubic, tetragonal, hexagonal, orthorhombic, and monoclinic phases.[11] Of these phases, the cubic phase is thermodynamically stable, whereas the monoclinic phase is metastable. Monoclinic Cu_2Se can convert into the thermodynamically more stable cubic Cu_2Se when the sample is heated to 133 °C.[12] Previously, several approaches have been developed to obtain copper selenides with different phase structures and properties.[13–17] For example, Zhang et al. synthesized hexagonal-phase CuSe nanosheets through a hot-injection method with $CuCl_2 \cdot 2H_2O$ as the Cu precursor and Se powder dissolved in a mixture of dodecanethiol and oleylamine as the Se precursor.[13] The obtained CuSe can be transformed into cubic-phase $Cu_{2-x}Se$ nanosheets simply by heat treatment in the presence of Cu^+ cations. Prieto et al. reported the synthesis of monoclinic Cu_2Se by a hot-injection method at 300 °C under inert conditions with octylphosphonic acid and trioctylphosphine as the solvents and copper acetate hydrate and Se powder as the reactants.[14] The obtained Cu_2Se nanoparticle thin film demonstrated high-performance tunable electronic properties through controlled oxidation. Recent studies have shown that metastable monoclinic Cu_2Se exhibits superior field-effect transistor and electrical performances and has promising applications.[16] Owing to the flexibility of the Cu_2Se family of compounds and the relatively difficult wet chemical synthesis of monoclinic Cu_2Se, reports on monoclinic Cu_2Se are rare.[14,15] Thus, the exploration of new and simple

[a] Jiangsu Collaborative Innovation Center of Biomedical Functional Materials, Jiangsu Key Laboratory of Biofunctional Materials, School of Chemistry and Materials Science, Nanjing Normal University,
Nanjing 210023, P. R. China
E-mail: daizhihuii@njnu.edu.cn
baojianchun@njnu.edu.cn
http://hky.njnu.edu.cn

Supporting information for this article is available on the WWW under http://dx.doi.org/10.1002/ejic.201500008.

phase-controlled synthetic strategies for the formation of Cu_2Se is desirable and could greatly extend the technological potential of Cu_2Se-based materials.

Surface-enhanced Raman scattering (SERS) spectroscopy has been extensively developed for its tremendous potential in chemical and biological sensing applications because of its high sensitivity, rapid response, and fingerprint effect.[18,19] The coinage metals (Ag, Au, and Cu) are good SERS substrates because of their high sensitivity, good reproducibility, and high enhancement factors (EFs). Recently, Pd-based nanostructures have been used as active substrates for SERS.[20,21] Comparatively, the SERS activities of semiconductor nanoparticles are much lower than those of metal nanostructures.[22–24] It is generally accepted that two main mechanisms contribute to the surface enhancement: the electromagnetic and the charge transfer mechanisms.[25,26] The former is a result of the large increase of the local electric field caused by the surface plasmon resonance of nanosized metal particles, whereas the latter involves charge transfer between the semiconductor and probe molecules[27–30] through chemisorption interactions. Thus, the combination of metal nanoparticles with semiconductors to form heterostructures is an effective approach to enhance SERS activity as a result of the synergetic effects between the components.[18,31,32] Several new types of hybrid SERS substrates, such as ZnO/Ag,[18,33] Ag_2S/Ag,[26] and Cu_2S/Ag,[32] have been prepared in recent years. Copper selenides exhibit particular optical, superionic, thermoelectric, and photoelectric properties and considerable progress has been made on their applications in electronic and optoelectronic devices.[16] However, no studies of the SERS performance of copper selenide based materials have been reported.

Herein, we report the synthesis of monoclinic Cu_2Se by simple and mild routes. In these routes, $[(C_2H_5)_4N]_2[CuCl_4]$, undecylenic acid (UA), and 1,3-dimethyl-3,4,5,6-tetrahydro-2(1*H*)-pyrimidinone (DMPU) were chosen as the copper source, capping reagent, and solvent, respectively. The Se^{-II} ions were generated from SeO_2 dissolved in terpineol instead of trioctylphosphine selenide (TOPSe). The Se^{-II} source was added to the $[(C_2H_5)_4N]_2[CuCl_4]$ solution through both "hot-injection" and "one-pot" methods at a moderate temperature (180 °C) to generate hexagonal CuSe and cubic $Cu_{2-x}Se$, respectively. Monoclinic Cu_2Se was readily obtained after the treatment of the CuSe or $Cu_{2-x}Se$ with trioctylphosphine (TOP) at 220 °C. The effects of certain reaction parameters on the formation of copper selenides were also investigated. The corresponding synthetic routes are shown in Scheme 1. By mixing the copper selenides (Cu_2Se, CuSe, or $Cu_{2-x}Se$) with $Pd(NO_3)_2$ in 2-propanol at room temperature, the corresponding copper selenide/Pd heterostructures were formed. We compared the SERS properties of these heterostructures with 4-mercaptopyridine (4-Mpy) as a probe molecule. The results indicated that the monoclinic Cu_2Se/Pd heterostructure possessed greater SERS performance than the other two copper selenide/Pd hybrids as well as the pure Pd and pure Cu_2Se. These results suggest that the heterostructures show phase- and composition-dependent characteristics and could have promising applications in chemical and biological detection.

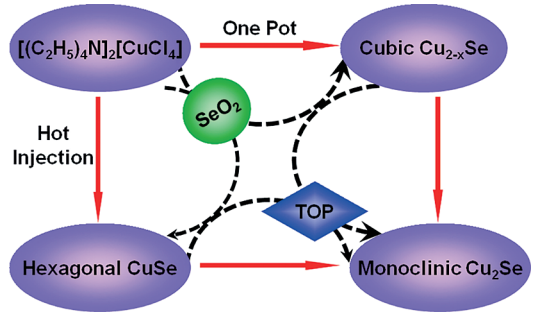

Scheme 1. Two simple routes for the fabrication of monoclinic Cu_2Se.

Results and Discussion

The energy-dispersive X-ray spectroscopy (EDS) spectra of the as-synthesized CuSe, $Cu_{2-x}Se$, and Cu_2Se are shown in Figure 1 (A–C), respectively. Except for small C and O peaks that originate from adsorbed organic capping reagents or air, only Cu and Se are detected. The Cu/Se atomic ratios of approximately 1:1, 1.8:1, and 2:1 in the three samples imply that they are CuSe, $Cu_{2-x}Se$, and Cu_2Se, respectively. Further evidence from the XRD analysis is shown in Figure 2. The diffraction peaks in Figure 2 (a) at 2θ = 26.4, 27.9, 30.9, 45.9, 49.9, and 56.5° can be indexed as the (101), (102), (006), (110), (108), and (116) faces of hexagonal CuSe (JCPDS 34-171), respectively, and the lattice parameters are calculated to be $a = b$ = 3.948 Å and c = 17.285 Å. In Figure 2 (b), the diffraction peaks at 2θ = 26.7, 30.9, 44.4, 52.6, 64.8, 71.3, and 82.1° can be assigned to the (111), (200), (220), (311), (400), (331), and (422) planes of cubic $Cu_{2-x}Se$, respectively, with the lattice parameters $a = b = c$ = 5.739 Å (JCPDS 6-680). A representative XRD pattern of the sample obtained by the heat treatment of CuSe or $Cu_{2-x}Se$ with TOP is shown in Figure 2 (c); the seven distinct diffraction peaks can be indexed as the (030), (400), (221), (610), (090), (012), and (422) planes of monoclinic Cu_2Se (JCPDS 27-1131) with the lattice parameters a = 14.807 Å, b = 20.481 Å, and c = 5.739 Å. Notably, no other impurities were found in the XRD analysis of Cu_2Se; therefore, both hexagonal-phase CuSe and cubic-phase $Cu_{2-x}Se$ can be converted completely to the monoclinic-phase Cu_2Se.

The morphologies of the three samples were examined by field emission SEM (FESEM). The FESEM image of CuSe in Figure 3 (A) shows that the crystals have a hexagonal platelike shape with a side length of 2–3 μm and a thickness of ca. 350 nm. From the FESEM image of $Cu_{2-x}Se$ in Figure 3 (B), we learn that the $Cu_{2-x}Se$ has a cubic morphology with a side length in the range 1.3–2.5 μm. Furthermore, these hexagonal or cubic crystals appear to be formed by the stacking of multiple slices (Figure S1 in the Supporting Information). The thicknesses of the slices

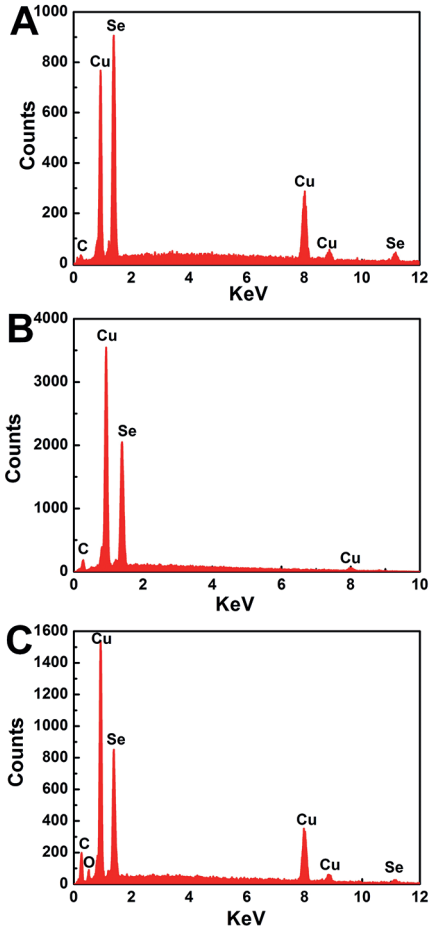

Figure 1. EDS spectra of the obtained (A) CuSe, (B) $Cu_{2-x}Se$, and (C) Cu_2Se.

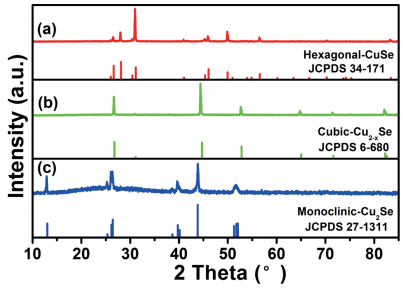

Figure 2. XRD patterns of obtained (a) hexagonal-phase CuSe, (b) cubic-phase $Cu_{2-x}Se$, and (c) monoclinic-phase Cu_2Se.

are ca. 80 nm for CuSe and 70 nm for $Cu_{2-x}Se$. The FESEM image of Cu_2Se obtained from the conversion of CuSe is shown in Figure 3 (C). By comparison with the CuSe image shown in Figure 3 (A), one point that should be noted after the heat treatment with TOP is that the hexagonal CuSe converts to monoclinic Cu_2Se with the retention of the size and morphology defined by the CuSe template. The main difference is that there are some small grains on the surface of the platelike Cu_2Se, which may result from the outward diffusion of the Cu_2Se formed by the conversion reaction of CuSe. A similar phenomenon occurs if $Cu_{2-x}Se$ is used as the template instead of CuSe. The chemical composition of these three samples were further characterized by elemental mapping (area scanning and line scanning) analysis (Figure 4). The results indicate that both Cu and Se are uniformly distributed throughout the crystals.

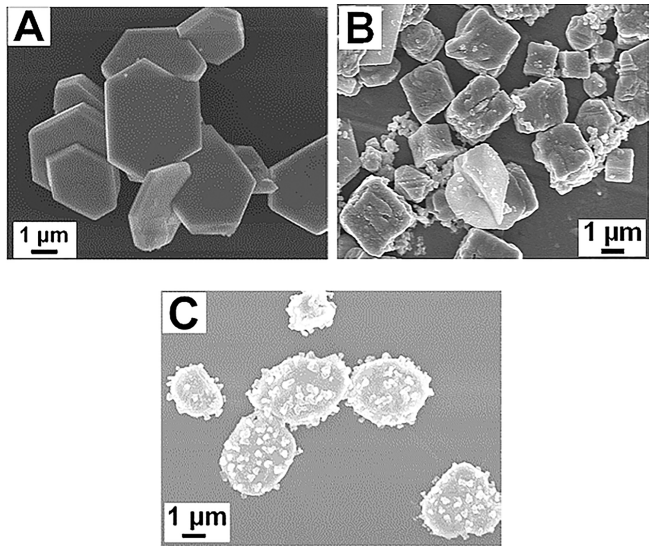

Figure 3. FESEM images of the obtained (A) CuSe, (B) $Cu_{2-x}Se$, and (C) Cu_2Se samples.

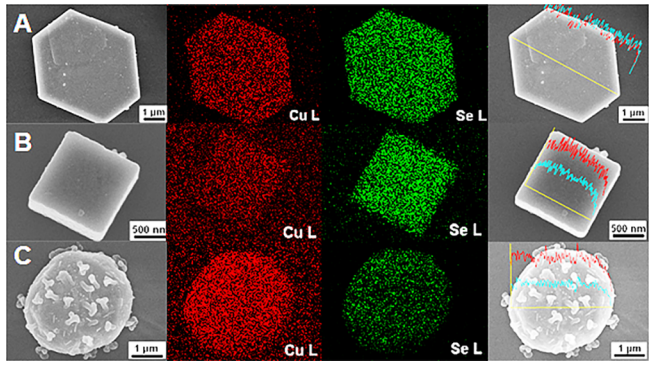

Figure 4. Element area and line scanning analysis of the obtained (A) CuSe, (B) $Cu_{2-x}Se$, and (C) Cu_2Se.

The preparation of selenides typically requires inert atmosphere protection because of their sensitivity to oxygen.[14] In the present strategy, although the experiments were conducted open to air, no oxide phases in the products were detected by the XRD analysis. This observation can be ascribed to the use of reductive UA and DMPU as solvents, and terpineol is also a reductant. In such a reductive reaction medium and with the UA acting as a capping molecule that forms a protective layer on the surface of the products, the selenides can be prepared in air with no additional protection.

As mentioned above, several approaches have been developed for the synthesis of copper selenides. However, the relationship between the product and the reaction conditions is irregular and remains to be clarified.[13,34,35] In the pres-

ent strategy, $[(C_2H_5)_4N]_2[CuCl_4]$ and SeO_2/terpineol were chosen as the copper and selenium sources, respectively. In the presence of UA and DMPU in a one-pot or hot-injection reaction mode, cubic $Cu_{2-x}Se$ or hexagonal CuSe formed. Why are two different copper selenides formed from the same reaction system by only changing the reaction mode? We speculate that the formation of $Cu_{2-x}Se$ or CuSe is mostly dependent on the redox reaction kinetics and the reaction time. The one-pot mode requires a longer reaction time than the hot-injection method. During the mixing of $[(C_2H_5)_4N]_2[CuCl_4]$ with SeO_2/terpineol solution in the hot-injection mode, the relatively low redox potential ($[CuCl_4]^{2-} \rightarrow Cu^{I}$) and shorter reaction time cause the precipitation reaction of $[CuCl_4]^{2-}$ ions with Se^{2-} ions to surpass the reduction reaction of $[CuCl_4]^{2-}$ ions with terpineol, and this leads to the formation of CuSe. Further evidence was obtained from the following experiments. If $CuCl_2$ or $CuSO_4$ is used instead of $[(C_2H_5)_4N]_2[CuCl_4]$ with the other conditions kept constant (hot-injection mode), $Cu_{2-x}Se$ is formed (Figure S2A and B). By doubling the amount of terpineol with the other conditions unchanged, a mixture of CuSe and $Cu_{2-x}Se$ is generated (Figure S2C). By further increasing the amount of terpineol (by four times), $Cu_{2-x}Se$ is obtained. It is reasonable that the oxidizing ability of the Cu^{2+} ions in $CuCl_2$ and $CuSO_4$ is stronger than that if the Cu^{2+} centers in $[(C_2H_5)_4N]_2[CuCl_4]$; thus, the reduction reaction of $CuCl_2$ or $CuSO_4$ with terpineol is the main reaction to yield $Cu_{2-x}Se$. Increased amounts of terpineol are beneficial for the reduction of Cu^{II} to form $Cu_{2-x}Se$; thus, when the precipitation reaction of the Cu^{II} species with Se^{2-} ions and the reduction of Cu^{II} by terpineol proceed simultaneously, a mixture of CuSe and $Cu_{2-x}Se$ forms. These results also imply that the preparation of CuSe and $Cu_{2-x}Se$ can be readily controlled by adjusting the amount of terpineol used.

Cubic- or tetragonal-phase Cu_2Se is typically obtained by the hot-injection,[14] single-source precursor,[15] or hydrothermal methods.[16] Additionally, Cu_2Se is prone to oxidation into more thermodynamically stable nonstoichiometric copper chalcogenide phases. In the present case, we used TOP as an extraction agent, reducing agent, and stabilizing agent and it can cause hexagonal CuSe and cubic $Cu_{2-x}Se$ to readily convert to monoclinic Cu_2Se at 220 °C. This process can be considered a viable nanoparticle "conversion chemistry" reaction. Although some selenium- or sulfur-rich metal chalcogenides, such as $NiSe_2$ and FeS_2, have been chemically transformed into the corresponding lower-chalcogen compounds (Ni_3Se_2 and FeS) through TOP treatment,[36,37] the fabrication of Cu_2Se from CuSe or $Cu_{2-x}Se$ as the starting material through this simple route has not been reported to date. In addition, compared to that of CuSe, the morphology of Cu_2Se changes slightly, possibly as a result of the following two factors. Firstly, the outward diffusion of generated Cu_2Se in the conversion process of CuSe makes the surface of Cu_2Se become coarser. The other factor is that the conversion of CuSe to Cu_2Se causes lattice expansion/contraction, which leads to the formation of quasicircle platelike crystals.

Copper selenide/Pd heterostructures were readily obtained by simply mixing copper selenides and $Pd(NO_3)_2$ in a 2-propanol solution; the 2-propanol acts as both the solvent and the reducing agent. The compositions of the composites were determined by EDS analysis (Figure S3). The EDS results clearly reveal the presence of Cu, Se, and Pd. The morphologies and microstructures of these three semiconductor–metal composites were investigated by TEM and HRTEM. To perform the TEM and HRTEM analyses and to gain information about the Pd nanoparticles on the surface of the copper selenides, the samples were sonicated for ca. 1 h to form slices. The TEM image of Cu_2Se/Pd is shown Figure 5 (A); most of the Pd particles are well dispersed on the surface of the sheetlike Cu_2Se. The HRTEM image of Cu_2Se/Pd (Figure 5, B) reveals that the Pd particles are mainly in the 4–8 nm range. Furthermore, two different sets of lattice fringes are clearly displayed. The lattice spacing of ca. 0.19 nm can be assigned to the (200) plane of cubic-phase Pd. The other lattice spacing of ca. 0.23 nm can be attributed to the (610) plane of hexagonal-phase Cu_2Se. In addition, it can be seen that these Pd nanocrystals grow epitaxially on the surface of the Cu_2Se to form the heterostructure; this may result in good structural stability, which would be beneficial for their practical application. As shown in Figure S4A–D, two sets of different lattice fringes (Figure S4B and D) indicate that the CuSe/Pd and $Cu_{2-x}Se$/Pd heterostructures are formed, respectively.

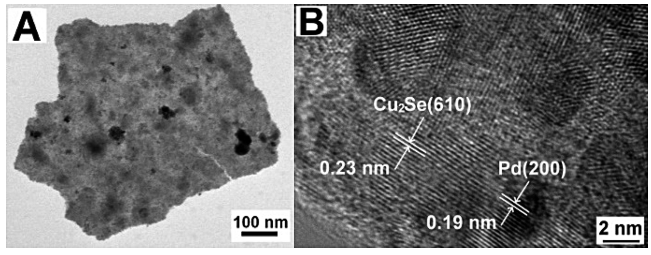

Figure 5. (A) TEM and (B) HRTEM images of the synthesized Cu_2Se/Pd.

The compositions of the copper selenide/Pd heterostructures were also examined by XPS analysis (Figure 6). As displayed in Figure 6 (A), the peaks located at binding energies of 931.64, 951.55, and 54.11 eV correspond to Cu 2p3/2, Cu 2p1/2, and Se 3d of the Cu_2Se/Pd, respectively; therefore, the valence of Cu is +1.[11] For CuSe/Pd, the peaks at binding energies of 932.27, 952.11, and 54.26 eV (Figure 6, B) are assigned to Cu 2p3/2, Cu 2p1/2, and Se 3d, respectively, in agreement with the literature values.[38] The binding energies of 931.85, 951.76, and 54.18 eV for $Cu_{2-x}Se$/Pd (Figure 6, C) are assigned to Cu 2p3/2, Cu 2p1/2, and Se 3d, respectively, and are similar to the literature values.[35] The binding energies at 338 eV in Figure 6 (A–C) are assigned to metallic Pd.[39,40] Therefore, the different binding energies of the Cu species in the three samples reveal the different valences of Cu. The high-resolution XPS scans for the Cu 2p, Se 3d, and Pd 3d cores are given in Figure S5.

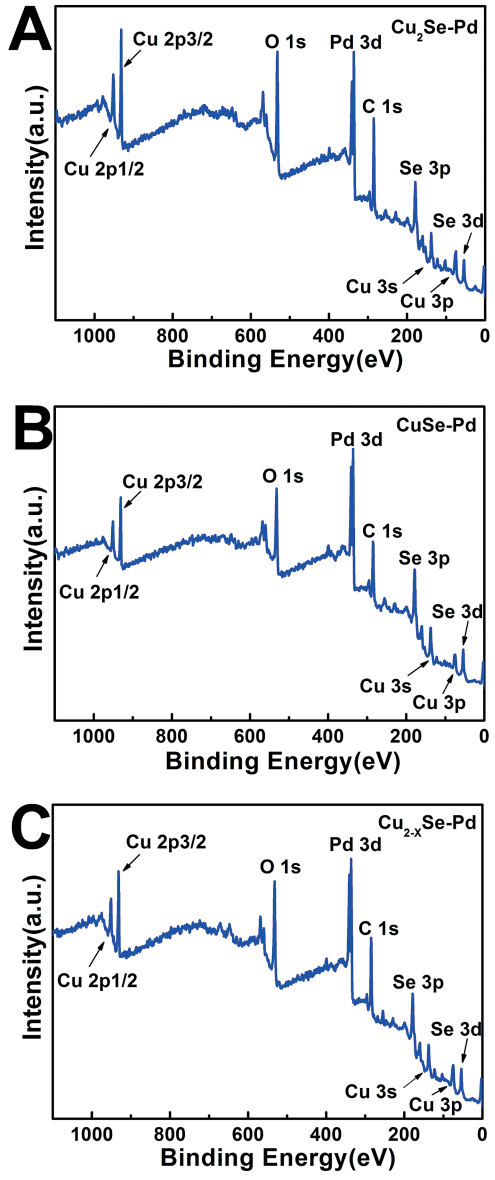

Figure 6. Full XPS spectra of (A) monoclinic-phase Cu_2Se/Pd, (B) hexagonal-phase CuSe/Pd, and (C) cubic-phase $Cu_{2-x}Se$/Pd.

SERS Detection of 4-Mercaptopyridine on Copper Selenide/Pd Heterostructures

The performance of the Cu_2Se/Pd heterostructures as SERS substrates was tested with 4-Mpy as a probe molecule. For comparison, the SERS performances of CuSe/Pd and $Cu_{2-x}Se$/Pd were also measured. The Raman spectra of 4-Mpy adsorbed on Cu_2Se/Pd, CuSe/Pd, and $Cu_{2-x}Se$/Pd, as well as that of 0.2 M 4-Mpy ethanol solution are shown in Figure 7 (A). The Raman intensity of 4-Mpy adsorbed on Cu_2Se/Pd is significantly enhanced relative to those of 4-Mpy adsorbed on the other two heterostructures. The SERS intensity of the Cu_2Se/Pd is nearly nine times higher than that of CuSe/Pd and six times higher than that of $Cu_{2-x}Se$/Pd at a wavenumber of 1591 cm^{-1}. The peak at $\tilde{\nu}$ = 1037 cm^{-1} is related to the pyridine ring C–H in-plane bending mode, whereas the band at $\tilde{\nu}$ = 1227 cm^{-1} is ascribed to the CH/NH deformation mode of 4-Mpy. The bands at $\tilde{\nu}$ = 1624 and 1591 cm^{-1} are assigned to the pyridine ring C=C stretching mode of 4-Mpy with protonated and deprotonated nitrogen atoms, respectively. It is worth noting that the appearance of the strongly enhanced band at $\tilde{\nu}$ = 1117 cm^{-1}, which corresponds to the ring-breathing/C–S stretching mode, indicates that 4-Mpy is adsorbed on the substrates through the sulfur atom. This is also supported by the C–S stretching mode at $\tilde{\nu}$ = 782 cm^{-1}, which displays an increase in intensity. To further ascertain the performance of the Cu_2Se/Pd component, the SERS spectra of 4-Mpy adsorbed on Cu_2Se and Pd were measured and are shown in Figure 7 (B). The SERS intensity of the Cu_2Se/Pd is nearly three times higher than that of pure Cu_2Se and six times higher than that of pure Pd at a wave-

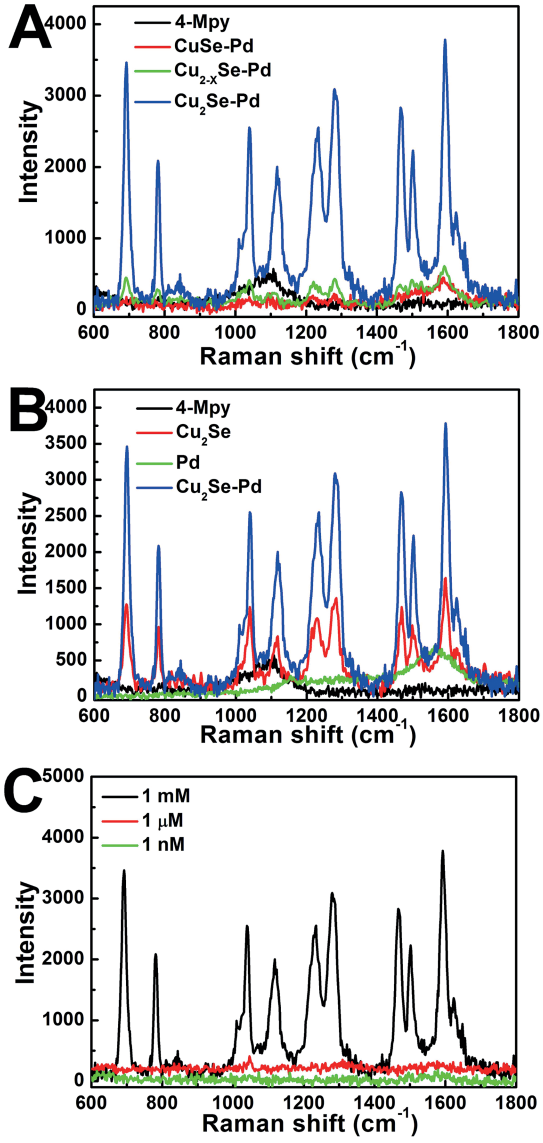

Figure 7. (A) SERS spectra of 4-Mpy adsorbed on films of Cu_2Se/Pd, CuSe/Pd, and $Cu_{2-x}Se$/Pd. (B) SERS spectra of 4-Mpy adsorbed on films of Cu_2Se, Pd, and Cu_2Se/Pd as well as that of 0.2 M 4-Mpy. (C) SERS spectra of 4-Mpy adsorbed on Cu_2Se/Pd with solutions ranging from 1×10^{-3} to 1×10^{-9} M.

number of 1591 cm^{-1}; these results demonstrate the excellent SERS performance of the heterostructure.

The large Raman intensity enhancement on the Cu_2Se/Pd heterostructure, compared with those of pure Cu_2Se and pure Pd, may result from the following factors. First, the enhancement can be readily attributed to the surface plasmon resonance of well-dispersed nanosized Pd particles ("hot spots") on the surface of Cu_2Se. Second, the enhancement may also result from charge transfer, including charge transfer between Pd and Cu_2Se and charge transfer between Cu_2Se and 4-Mpy molecules. Moreover, the junctions between positively charged Pd particles and negatively charged Cu_2Se may induce a stronger electromagnetic field; thus, the Pd would excite a more intense localized surface plasmon resonance under the irradiation of a suitable laser, and this would lead to the enhancement of the SERS signals of 4-Mpy molecules adsorbed on the Cu_2Se through this long-range electromagnetic enhancement. In short, these strong synergistic effects between the Cu_2Se and Pd are beneficial for the SERS enhancement. In addition, as seen from the commonly observed crystal structures of monoclinic-phase Cu_2Se, hexagonal-phase CuSe, and cubic-phase $Cu_{2-x}Se$ (Scheme 2), the Cu coordination number (CN) in monoclinic Cu_2Se (CN = 5) is distinct from those in the other two copper selenides (CN = 4). This leads to the strongest interaction between Cu_2Se and 4-Mpy because of the coordination of Cu with S; consequently, Cu_2Se displays the strongest Raman intensity enhancement. It is also necessary to note that the Cu_2Se/Pd heterostructure exhibits better SERS performance than other substrates such as Pd, Pt,[41,42] ZnS,[43] and CuO,[44].

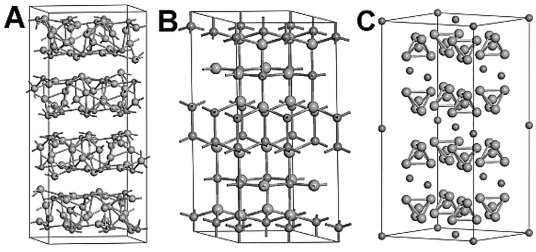

Scheme 2. The commonly observed crystal structures of (A) monoclinic-phase Cu_2Se, (B) hexagonal-phase CuSe, and (C) cubic-phase $Cu_{2-x}Se$.

The SERS enhancement factor (EF) of the substrate is an important number for characterization of the SERS effect. We calculated the EF to quantify the SERS enhancement of the probe molecules adsorbed on the Cu_2Se/Pd substrate. The EF can be estimated from Equation (1).[45]

$$EF = (I_{SERS}/I_{bulk}) \times (N_{bulk}/N_{SERS}) \quad (1)$$

N_{bulk} and N_{SERS} are numbers of molecules exposed to laser irradiation in the normal Raman and SERS spectra, respectively, and I_{SERS} and I_{bulk} are the measured intensities of the same mode in the SERS spectra of the 4-Mpy molecules on the surface of the Cu_2Se/Pd substrate and the normal spectra of bulk 4-Mpy powder, respectively. The symmetric vibrational band observed at $\tilde{\nu}$ = 1591 cm^{-1} was used to determine the EF. The I_{surf} and I_{bulk} were observed to be 3800 and 6165 counts, respectively (Figure S6A). The total number of molecules for 10 mg of 4-Mpy powder was calculated to be 5.41×10^{19}. According to the 2 μm diameter of the laser beam spot, N_{bulk} was obtained as 4.42×10^{12}. For N_{SERS}, we assume that all 4-Mpy molecules are adsorbed on the substrate in a single layer. Moreover, if all of the 4-Mpy is adsorbed on Cu_2Se/Pd, the maximum concentration of 4-Mpy is 1.0×10^3 M. The area of molecules participating in the scattering process is essentially determined by the 2 μm diameter of the laser beam spot. During the experiment, 4-Mpy (10 μL, 1.0×10^3 M) was dropped on the surface of the sampling area (ca. 6 mm in diameter). We estimated the total number of 4-Mpy molecules adsorbed on the Cu_2Se/Pd to be 6.02×10^{15}. Taking the laser spot size (ca. 2 μm in diameter) into account, the value of N_{SERS} is 6.69×10^8. Thus, the EF is estimated to be ca. 4.1×10^3.

The sensitivity of the Cu_2Se/Pd heterostructure was tested for various concentrations of 4-Mpy solution dropped onto the sample. As shown in Figure 7 (C), the intensity decreases as the 4-Mpy concentration decreases. However, at a 4-Mpy concentration as low as 1.0×10^{-9} M, four important bands at $\tilde{\nu}$ = 624, 1028, 1288 and 1555 cm^{-1} of 4-Mpy can still be identified (Figure S6B). In other words, the minimum detectable concentration is ca. 1.0×10^{-9} M.

Conclusions

This study presents a simple approach to the fabrication of monoclinic Cu_2Se. Hexagonal CuSe and cubic $Cu_{2-x}Se$ were prepared by the reaction of $[(C_2H_5)_4N]_2[CuCl_4]$ with SeO_2/terpineol in "hot-injection" and "one-pot" modes, respectively. They can then be readily converted to monoclinic Cu_2Se by treatment with TOP. Control experiments showed that the phase-selective synthesis of copper selenides can be realized by controlling the amount of terpineol used in the reaction. To the best of our knowledge, such a terpineol-based phase-control method has not been reported previously. Furthermore, with 2-propanol as both the solvent and the reducing agent, copper selenide/Pd heterostructures are readily produced. Owing to strong synergistic effects and phase-dependent characteristics, the SERS performance of the Cu_2Se/Pd heterostructure is superior to those of Cu_2Se, Pd, CuSe/Pd, and $Cu_{2-x}Se$/Pd as well as those of some other reported substrates. We expect that this synthetic strategy will help in the design and preparation of advanced chalcogenides and, thus, enable greater exploitation of their unique properties and potential applications.

Experimental Section

Materials: Tetraethylammonium chloride (98%) and trioctylphosphine (90%) were purchased from Aladdin. Undecylenic acid (95%), terpineol (95%), absolute alcohol, 2-propanol, and 4-Mpy

were obtained from Sinopharm Chemical Reagent Co. Ltd. Palladium(II) nitrate hydrate (99.8%) and DMPU (98%) were purchased from Alfa Aesar. Selenium dioxide (98%) and cupric chloride dihydrate (99.0%) were obtained from Shanghai Meixing Chemical Reagent Co. Ltd. All reagents were used as received without further purification.

$[(C_2H_5)_4N]_2[CuCl_4]$: In a typical synthesis, $CuCl_2{\cdot}2H_2O$ (0.85 g) was dispersed in absolute ethanol (5 mL), and this solution was marked as solution A. Likewise, $(C_2H_5)_4NCl{\cdot}H_2O$ (1.84 g) was dissolved in absolute ethanol (5 mL), and this solution was labeled solution B. Next, solution B was mixed with solution A, and the mixture was then heated to boiling for several minutes. The resulting bright yellow precipitate was collected by filtration and then dried under vacuum before use for the following syntheses. $C_{16}H_{40}Cl_4CuN_2$ (465.87): calcd. C 41.25, H 8.66, N 6.01; found C 41.54, H 8.38, N 5.98.

Pure Hexagonal-Phase CuSe: $[(C_2H_5)_4N]_2[CuCl_4]$ (0.24 g, 0.5 mmol) was mixed with UA (1 mL) and DMPU (10 mL) in a 100 mL three-neck flask. Then, the reaction mixture was heated to 180 °C at a rate of 5 °C min^{-1} and maintained at that temperature for 30 min. Subsequently, the Se^{-II} precursor solution, obtained by dissolving SeO_2 (0.056 g) in terpineol (5 mL), was quickly injected into the $[(C_2H_5)_4N]_2[CuCl_4]$ solution. After 180 °C for 1 h, the reaction mixture was naturally cooled to room temperature. The crude product was separated by centrifugation and washed with absolute ethanol four or five times to remove the byproducts. Finally, the precipitate was dried in vacuo and used for further characterization and analysis.

Pure Cubic-Phase $Cu_{2-x}Se$: The synthetic procedure and post-treatment steps of cubic-phase $Cu_{2-x}Se$ were similar to those for the synthesis of pure hexagonal-phase CuSe; the only difference was the addition of the reactants. The CuSe was obtained by the hot-injection method, whereas the $Cu_{2-x}Se$ was achieved by the one-pot method.

Pure Monoclinic-Phase Cu_2Se: In a typical synthesis of Cu_2Se, CuSe (0.02 g) or $Cu_{2-x}Se$ was mixed with TOP (12 mL) in a 50 mL three-neck flask. Then, the reaction mixture was heated to 220 °C at a rate of 5 °C min^{-1} and maintained at that temperature for 60 min. Afterward, the reaction mixture was naturally cooled to room temperature. The supernatant was discarded, and the precipitate was redispersed in hexane/absolute ethanol (5 mL) and subjected to centrifugation at 12000 rpm for 10 min several times. Finally, the product was dried and stored under vacuum for subsequent characterization and analysis.

Cu_2Se/Pd, $Cu_{2-x}Se$/Pd, and CuSe/Pd Heterostructures: A typical synthetic procedure for Cu_2Se/Pd is briefly described. In a 100 mL three-neck flask, Cu_2Se (0.103 g, 0.5 mmol) and $Pd(NO_3)_2{\cdot}2H_2O$ (0.021 g) were mixed with 2-propanol (15 mL). The dark brown reaction mixture was stirred for 30 min at room temperature. The product was precipitated by centrifugation and washed with absolute ethanol several times. Finally, the product was dried and stored under vacuum for characterization and analysis.

The synthetic procedure and post-treatment steps for CuSe/Pd and $Cu_{2-x}Se$/Pd were similar to those for the synthesis of Cu_2Se/Pd.

Characterization: The XRD patterns of powder samples were recorded in the 2θ range 10 to 90° with a D/max 2500 VL/PC diffractometer (Japan) equipped with a graphite-monochromated Cu-K_α radiation source (λ = 1.54060 Å). The corresponding work voltage and current were 40 kV and 100 mA, respectively. The MDI Jade 5.0 software was used to process the acquired diffraction data. The EDS spectra were obtained with a JSM-5610LV-Vantage spectrometer. Elemental analyses were performed with a Vario EL III element analyzer. The XPS data were acquired with a scanning X-ray microprobe (PHI 5000 Verasa, Ulacphi, Inc.) and with Al-K_α radiation. The Cu 2p, Se 3d, and Pd 3d binding energies were calibrated by using the C 1s peak (BE = 284.6 eV) as a standard. The FESEM images were obtained with an ultrahigh-resolution thermal emission scanning electron microscope (JSM-7600F, Japan), operated at an accelerating voltage of 10 kV. The transmission electron microscopy (TEM) images were acquired with a JEM-200CX instrument (Japan) at an accelerating voltage of 200 kV. The HRTEM images were obtained with a JEOL-2100F apparatus at an accelerating voltage of 200 kV with STEM and EDS detectors, which could be used for elemental mapping analysis. The Raman spectra were recorded with a JY HR 800 (France) instrument with an optical multichannel Microdil 28 (Dilor) spectrometer equipped with a microscope. An objective lens with ×100 magnification was used both for focusing the excitation light (Ar^+ laser, 514.5 nm) and for collecting the scattered light.

SERS Measurements: The sample (5 mg) was placed on a Si wafer, which was then pressed with another Si wafer to form a circle with a diameter of ca. 5 mm. Next, a 4-Mpy (10.0 μL) aqueous solution at the required concentration (1.0×10^{-3} to 1.0×10^{-9} M) was dropped onto the sample, which was dried at room temperature. The SERS measurements were conducted with a confocal microprobe Raman system with an excitation wavelength of 514.5 nm. During the SERS measurements, the laser light was vertically projected onto the samples at a power of 3 mW with a resultant beam diameter of ca. 2 μm.

Acknowledgments

This work was supported by the National Natural Science Foundation of China (NSFC) (grant numbers 21175069, 21171096, 21475062 and 21471081) and the Research Fund for the Doctoral Program of Higher Education of China (grant number 20113207110005). The authors greatly appreciate the financial support from the Priority Academic Program Development of Jiangsu Higher Education Institutions.

[1] M. R. Gao, Y. F. Xu, J. Jiang, S. H. Yu, *Chem. Soc. Rev.* **2013**, *42*, 2986–3017.
[2] P. V. Kamat, K. Tvrdy, D. R. Baker, J. G. Radich, *Chem. Rev.* **2010**, *110*, 6664–6688.
[3] P. P. Wang, H. Y. Sun, Y. J. Ji, W. H. Li, X. Wang, *Adv. Mater.* **2014**, *26*, 964–969.
[4] J. D. Marshall, M. J. Schnitzer, *ACS Nano* **2013**, *7*, 4601–4609.
[5] Y. Wang, Y. N. Ni, *Anal. Chem.* **2014**, *86*, 7463–7470.
[6] Y. Zhang, C. G. Hu, C. H. Zheng, Y. Xi, B. Y. Wan, *J. Phys. Chem. C* **2010**, *114*, 14849–14853.
[7] J. P. Heremans, V. Jovovic, E. S. Toberer, A. Saramat, K. Kurosaki, A. Charoenphakdee, S. Yamanaka, G. J. Snyder, *Science* **2008**, *321*, 554–557.
[8] D. Bräuhaus, C. Schindler, U. Böttger, R. Waser, *Thin Solid Films* **2008**, *516*, 1223–1226.
[9] D. Chun, R. M. Walser, R. W. Bené, T. H. Courtney, *Appl. Phys. Lett.* **1974**, *24*, 479–481.
[10] D. P. Li, Z. Zheng, Y. Lei, S. X. Ge, Y. D. Zhang, Y. G. Zhang, K. W. Wong, F. L. Yang, W. M. Lau, *CrystEngComm* **2010**, *12*, 1856–1861.
[11] S. L. Liu, Z. S. Zhang, J. C. Bao, Y. Q. Lan, W. W. Tu, M. Han, Z. H. Dai, *J. Phys. Chem. C* **2013**, *117*, 15164–15173.
[12] H. Chi, H. Kim, J. C. Thomas, G. S. Shi, K. Sun, M. Abeykoon, E. S. Bozin, X. Y. Shi, Q. Li, X. Shi, E. Kioupakis, A. Van der Ven, M. Kaviany, C. Uher, *Phys. Rev. B* **2014**, *89*, 195209.

[13] X. J. Wu, X. Huang, J. Q. Liu, H. Li, J. Yang, B. Li, W. Huang, H. Zhang, *Angew. Chem. Int. Ed.* **2014**, *53*, 5083–5087.
[14] S. C. Riha, D. C. Johnson, A. L. Prieto, *J. Am. Chem. Soc.* **2011**, *133*, 1383–1390.
[15] K. H. Low, C. H. Li, V. A. L. Roy, S. S. Y. Chui, S. L. F. Chan, C. M. Che, *Chem. Sci.* **2010**, *1*, 515–518.
[16] J. B. Zhu, Q. Y. Li, L. F. Bai, Y. F. Sun, M. Zhou, Y. Xie, *Chem. Eur. J.* **2012**, *18*, 13213–13221.
[17] C. M. Hessel, V. P. Pattani, M. Rasch, M. G. Panthani, B. Koo, J. W. Tunnell, B. A. Korgel, *Nano Lett.* **2011**, *11*, 2560–2566.
[18] H. B. Tang, G. W. Meng, Q. Huang, Z. Zhang, Z. L. Huang, C. H. Zhu, *Adv. Funct. Mater.* **2012**, *22*, 218–224.
[19] K. Lee, V. P. Drachev, J. Irudayaraj, *ACS Nano* **2011**, *5*, 2109–2117.
[20] Y. J. Xiong, J. M. McLellan, J. Y. Chen, Y. D. Yin, Z.-Y. Li, Y. N. Xia, *J. Am. Chem. Soc.* **2005**, *127*, 17118–17127.
[21] J. F. Huang, Y. H. Zhu, M. Lin, Q. X. Wang, L. Zhao, Y. Yang, K. X. Yao, Y. Han, *J. Am. Chem. Soc.* **2013**, *135*, 8552–8561.
[22] Z. Q. Tian, B. Ren, D. Y. Wu, *J. Phys. Chem. B* **2002**, *106*, 9463–9483.
[23] A. Musumeci, D. Gosztola, T. Schiller, N. M. Dimitrijevic, V. Mujica, D. Martin, T. Rajh, *J. Am. Chem. Soc.* **2009**, *131*, 6040–6041.
[24] X. Q. Fu, F. L. Bei, X. Wang, X. J. Yang, L. D. Lu, *J. Raman Spectrosc.* **2009**, *40*, 1290–1295.
[25] T. Ming, L. Zhao, Z. Yang, H. J. Chen, L. D. Sun, J. F. Wang, C. H. Yan, *Nano Lett.* **2009**, *9*, 3896–3903.
[26] X. Q. Fu, T. S. Jiang, Q. Zhao, H. B. Yin, *J. Raman Spectrosc.* **2012**, *43*, 1191–1195.
[27] H. L. Liu, Z. L. Yang, L. Y. Meng, Y. D. Sun, J. Wang, L. B. Yang, J. H. Liu, Z. Q. Tian, *J. Am. Chem. Soc.* **2014**, *136*, 5332–5341.
[28] M. Dendisová, L. Havránek, M. Ončák, P. Matějka, *J. Phys. Chem. C* **2013**, *117*, 21245–21253.
[29] S. Ma, R. Livingstone, B. Zhao, J. R. Lombardi, *J. Phys. Chem. Lett.* **2011**, *2*, 671–674.
[30] B. N. Khlebtsov, V. A. Khanadeev, M. Y. Tsvetkov, V. N. Bagratashvili, N. G. Khlebtsov, *J. Phys. Chem. C* **2013**, *117*, 23162–23171.
[31] Y. X. Wang, W. Song, W. D. Ruan, J. X. Yang, B. Zhao, J. R. Lombardi, *J. Phys. Chem. C* **2009**, *113*, 8065–8069.
[32] W. Song, J. J. Wang, Z. Mao, W. Q. Xu, B. Zhao, *Spectrochim. Acta Part A* **2011**, *79*, 1247–1250.
[33] X. He, H. Wang, Q. Zhang, Z. B. Li, X. C. Wang, *Eur. J. Inorg. Chem.* **2014**, 2432–2439.
[34] Y. Liu, Q. F. Dong, H. T. Wei, Y. Ning, H. Z. Sun, W. J. Tian, H. Zhang, B. Yang, *J. Phys. Chem. C* **2011**, *115*, 9909–9916.
[35] S. Deka, A. Genovese, Y. Zhang, K. Miszta, G. Bertoni, R. Krahne, C. Giannini, L. Manna, *J. Am. Chem. Soc.* **2010**, *132*, 8912–8914.
[36] I. T. Sines, R. E. Schaak, *J. Am. Chem. Soc.* **2011**, *133*, 1294–1297.
[37] K. D. Oyler, X. L. Ke, I. T. Sines, P. Schiffer, R. E. Schaak, *Chem. Mater.* **2009**, *21*, 3655–3661.
[38] X. D. Liu, X. C. Duan, P. Peng, W. J. Zheng, *Nanoscale* **2011**, *3*, 5090–5095.
[39] X. Y. Li, X. Wang, S. Y. Song, D. P. Liu, H. J. Zhang, *Chem. Eur. J.* **2012**, *18*, 7601–7607.
[40] F. Niu, S. Q. Li, Y. C. Zong, Q. Yao, *J. Phys. Chem. C* **2014**, *118*, 19165–19171.
[41] M. E. Abdelsalam, S. Mahajan, P. N. Bartlett, J. J. Baumberg, A. E. Russell, *J. Am. Chem. Soc.* **2007**, *129*, 7399–7406.
[42] Z. Liu, Z. L. Yang, L. Cui, B. Ren, Z. Q. Tian, *J. Phys. Chem. C* **2007**, *111*, 1770–1775.
[43] Y. F. Wang, Z. H. Sun, H. L. Hu, S. Y. Jing, B. Zhao, W. Q. Xu, C. Zhao, J. R. Lombardi, *J. Raman Spectrosc.* **2007**, *38*, 34–38.
[44] Y. F. Wang, H. L. Hu, S. Y. Jing, Y. X. Wang, Z. H. Sun, B. Zhao, C. Zhao, J. R. Lombardi, *Anal. Sci.* **2007**, *23*, 787–791.
[45] C. J. Orendorff, A. Gole, T. K. Sau, C. J. Murphy, *Anal. Chem.* **2005**, *77*, 3261–3266.

Received: March 4, 2015
Published Online: March 25, 2015

